Resilient Respiration Rate Monitoring with Realtime Bimodal CSI Data

Xuyu Wang, *Member, IEEE*, Chao Yang, *Student Member, IEEE*, and Shiwen Mao, *Fellow, IEEE*

***Abstract*—Vital signs, such as respiration rate, can provide useful information for personal healthcare. In this paper, we present ResBeat, a commodity 5 GHz WiFi based system to exploit bimodal channel state information (CSI), including amplitude and phase difference, for realtime, long-term, and contact-free respiration rate monitoring. Specifically, we first present an analysis of breathing signal anomalies based on bimodal CSI data. Then, we present the design of the data preprocessing, adaptive signal selection, and breathing signal monitoring modules of ResBeat, and employ peak detection to estimate respiration rates. We conduct extensive experiments on respiration rate monitoring under three different environments, where superior performance over two alternative methods is demonstrated.**

***Keywords*—5GHz WiFi, Bimodal data, Channel state information (CSI), Healthcare, Internet of Things (IoT), Vital sign monitoring.**

I. Introduction

Vital signs of a patient can provide useful clues to many diseases such as heart disease, lung disorder, and diabetes, which cost huge expenses for treatment [1], [2]. For instance, monitoring breathing signals can help a patient to detect sleep disorders or anomalies, and prevent sudden infant death syndrome (SIDS) of sleeping infants [3]. To provide effective cure for such diseases, measurements of human respiratory rate over an extended period of time (e.g., daily) are becoming increasingly important. However, conventional breathing rate measurement methods include counting manually with a stethoscope or using a specific device such as a capnography [4], which are both inconvenient to use and discomfort for patients. Furthermore, a patient being monitored may intentionally reduce the respiration rate or breath more smoothly, leading to inaccurate results. Effective solutions are in great demand for realtime, long-term, and unobtrusive respiration signal monitoring [5], [6].

To this end, several contact-free vital signal monitoring systems have been proposed in the literature, which mainly leverage RF signals to detect the chest movements caused by respiration. For example, Vital-Radio can measure breathing and heart rates for multiple people simultaneously using a frequency modulated continuous wave (FMCW) radar [7]. Another system, mmVital, detects the received signal strength (RSS) of 60 GHz millimeter wave (mmWave) signals to estimate respiratory rate and heart rate [8]. Both systems operate on a wide spectrum with specially designed hardware. Moreover, some other techniques, such as Doppler radar [9] and ultra-wideband radar [10], can also monitor vital signs, but also require dedicated hardware at high frequency, resulting in relatively higher costs. Finally, Ubibreathe is implemented with off-the-shelf WiFi devices, and uses RSS at a WiFi device attached to a patient's chest for breathing detection [11]. It requires the person to be situated on the line-of-sight (LOS) path between the device and the WiFi access point.

Unlike RSS, channel state information (CSI) provides fine-grained physical layer (PHY) information, which can be extracted from open-source device drivers for several WiFi cards, e.g., the Intel WiFi Link 5300 NIC [12] and the Atheros AR9580 chipset [13]. CSI can reveal the channel characteristics experienced by the received signal, including multipath effect and shadow fading. Moreover, CSI data is a more stable representation of channel characteristics, including amplitude and phase information of subcarrier-level measurements in the orthogonal frequency division multiplexing (OFDM) system. Recently, a CSI amplitude based method is proposed for measuring respiration and heart beats when a person is sleeping [14]. In addition, our recent works PhaseBeat [15], [16] and TensorBeat [17] leverage CSI phase difference data to monitor a single person's vital signals and multiple persons' respiration signals, respectively. However, these works are not effective in detecting the weak respiration signal at some special locations [18], which motivates us to use bimodal CSI data for resilient breathing monitoring.

In this paper, we exploit CSI bimodal data, including amplitude and phase difference, to detect and monitor breathing signals with commodity 5GHz WiFi devices. For indoor environments under small-scale fading, we consider the chest reflected signal as a *dynamic component*, while lumping the line-of-sight (LOS) and all other multipath signals together into a *static component*. We model the amplitude and phase responses on the OFDM subcarriers with the dynamic and static component approach, and prove that CSI amplitude and phase information carry the breathing information with the same rate. Moreover, we present an analysis of breathing signal anomalies with CSI amplitude and phase information, and show that the breathing signals can be weak at some monitoring locations (i.e., corner cases). Thus, we propose to use bimodal CSI data for resilient respiration monitoring,

This work is supported in part by the NSF under Grant ECCS-1923163 and through the Wireless Engineering Research and Education Center (WEREC) at Auburn University. An earlier version of this paper was presented at IEEE Globecom 2017, Singapore, Dec. 2017. The conference version can be found at: https://ieeexplore.ieee.org/document/8255021.

X. Wang is with the Department of Computer Science, California State University, Sacramento, CA 95819-6021, USA. C. Yang and S. Mao are with the Department of Electrical and Computer Engineering, Auburn University, Auburn, AL 36849-5201, USA. Email: xuyu.wang@csus.edu, czy0017@tigermail.auburn.edu, smao@ieee.org.

Digital Object Identifier 10.1109/JSEN.2020.2989780

motivated by the fact that CSI amplitude and phase difference data in consecutively received packets are stable, and they are complementary to each other with respect to mitigating the anomalous respiration signals at some bad locations. The bimodal data is also robust to environment interference and body movements for respiration signal monitoring.

We present the design of ResBeat, i.e., **Res**ilient realtime breathing **Beat** monitoring with bimodal CSI amplitude and phase difference data with commodity WiFi devices. The ResBeat system consists of data preprocessing, adaptive signal selection, and breathing signal monitoring modules. In the data preprocessing module, we calibrate CSI data with an *exponentially weighted moving average* (EWMA) method to extract the static, or environment, component and the dynamic, or breathing, component. For adaptive signal selection, we propose a signal selection algorithm based on signal energy detection and movement detection, to select the most sensitive signal group, which can successfully mitigate the effect of anomalous respiration signals. Finally, peak detection is applied to estimate breathing rates in realtime CSI data.

We implement ResBeat with commodity 5GHz WiFi devices and evaluate its performance with four persons over a period of three months in different indoor environments, such as a computer laboratory, a through-wall scenario, and a long corridor scenario. The results validate that the ResBeat system can achieve high estimation accuracy of breathing rate: the median error is 0.25 bpm (breaths per minute), and has a higher success rate of 90% for respiration rate detection at different locations. The main contributions of this paper are summarized in the following.

- We theoretically verify the feasibility of using *bimodal* CSI data for respiration monitoring. In particular, we provide a breathing signal anomaly analysis based on CSI amplitude and phase information. To the best of knowledge, this work, first presented in part in [1], was the first to leverage *bimodal* realtime CSI amplitude and phase difference data to improve the robustness of respiration rate measurement.
- We design and implement the data preprocessing, adaptive signal selection, and breathing signal monitoring modules to process the collected bimodal CSI data in ResBeat. We employ the EWMA method to obtain the environment component and the breathing component. Moreover, we utilize the peak detection method for respiration rate estimation.
- We prototype the ResBeat design with commodity 5 GHz WiFi devices and validate its superior performance in three typical indoor environments with extensive experiments. The experimental results demonstrate that the ResBeat system can achieve higher success rates than an amplitude based method and a phase difference based method for respiration monitoring.

The remainder of this paper is organized as follows. The preliminaries and breathing signal anomaly analysis are presented in Section II. We design the ResBeat system in Section III and validate its performance in Section IV. Section V review related work and Section VI summaries this paper.

II. Preliminaries and Breathing Signal Anomaly Analysis

A. Channel State Information Preliminaries

Many modern wireless network standards (e.g., WiFi, LTE, WiMAX, DVB) adopt OFDM for data transmission, which is proper for frequency selective channels and achieves high data rates. For OFDM, the total spectrum is divided into multiple orthogonal, narrowband, subcarriers. By leveraging Inverse fast Fourier transform (IFFT), data can be transmitted on the subcarriers to alleviate channel fading caused by large delay spreads. Moreover, the cyclic redundancy is used to reduce the complexity of fast Fourier transform (FFT) processing at the receiver. Using the device driver for off-the-shelf NICs, such as the Intel WiFi Link 5300 NIC [12] and the Atheros AR9580 chipset [13], we can obtain CSI data from the subcarriers for each received WiFi packet, which represent the wireless channel characteristics such as the shadow fading, distortion and multipath effect.

For ResBeat, we use Intel 5300 NIC to obtain CSI data, which report 30 out of the 56 subcarriers at the WiFi receiver for a 20 MHz or 40 MHz channel. The channel frequency response of subcarrier i, H_i, is a complex value, that is

$$\mathrm{H}_i = |\mathrm{H}_i| \exp(j\angle \mathrm{H}_i), \tag{1}$$

where $|\mathrm{H}_i|$ and $\angle \mathrm{H}_i$ are the amplitude and phase responses of subcarrier i, respectively.

B. Respiration Signal Anomaly Analysis

Consider an indoor environment with NLOS components [19], [20], where a WiFi transmitter transmits a packets. The WiFi signal propagates in all directions, including a signal hits the chest of the patient and reflected by the chest. The receiver receives the chest reflected signal, along with many other multipath components. Assume there is no other movements in the room. The chest reflected signal is regarded as the *dynamic component*, and the sum of the LOS and all other multipath signals is regarded as a *static component*. The frequency response of subcarrier i, denoted by H_i, can be written as

$$\begin{aligned}\mathrm{H}_i &= \sum_{k=0,k\neq d}^{K} h_k \cdot \exp\{-j2\pi f_i \xi_k\} + h_d \cdot \exp\{-j2\pi f_i \xi_d\} \\ &= \mathrm{H}_i^s + \mathrm{H}_i^d = |\mathrm{H}_i^s| \exp(j\angle \mathrm{H}_i^s) + |\mathrm{H}_i^d| \exp\left(j\angle \mathrm{H}_i^d\right), \end{aligned} \tag{2}$$

where K is the number of multipath components, h_k and ξ_k are the attenuation and propagation delay of the kth path, respectively; $\mathrm{H}_i^s = \sum_{k=0,k\neq d}^{K} h_k \cdot \exp\{-j2\pi f_i \xi_k\}$ is the static component and $\mathrm{H}_i^d = h_d \cdot \exp\{-j2\pi f_i \xi_d\}$ is the dynamic component, and $|\cdot|$ and $\angle(\cdot)$ are the amplitude and phase, respectively,

The amplitude response of subcarrier i can be computed as

$$|\mathrm{H}_i| = \sqrt{|\mathrm{H}_i^s|^2 + |\mathrm{H}_i^d|^2 + 2|\mathrm{H}_i^s||\mathrm{H}_i^d| \cos\left(\angle \mathrm{H}_i^s - \angle \mathrm{H}_i^d\right)}. \tag{3}$$

In (3), the amplitude and phase of the static component H_i^s are regarded as constants, and the amplitude of the dynamic component H_i^d is also assumed to be constant, given that there

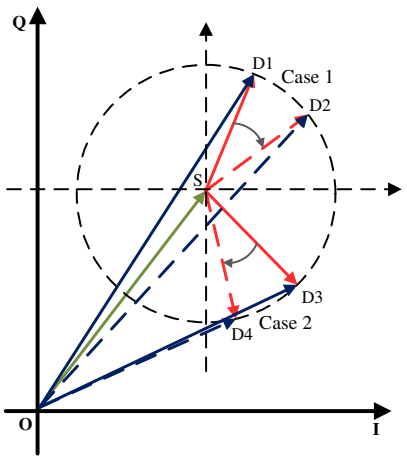

Fig. 1. The geometric relationship of the static and dynamic components of a received WiFi signal, for respiration signal anomaly analysis.

is no other movements in the neighborhood. Moreover, the phase of the dynamic component H_i^d can be modeled as

$$\angle \mathrm{H}_i^d = \frac{2\pi L}{\lambda_i} = \frac{2\pi(L_0 + \ell \cdot \cos(2\pi f_b t))}{\lambda_i}, \tag{4}$$

where λ_i is the wavelength of subcarrier i, $L = L_0 + \ell \cdot \cos(2\pi f_b t)$ is the distance and L_0 is the average distance of the chest-reflection path, respectively, ℓ is the amplitude and f_b is the frequency of chest movement. Note that the phase of the dynamic component H_i^d is periodic because the dynamic path distance L is periodic due to chest movements (i.e., it gets slightly longer when exhaling and shorter when inhaling). Thus, the amplitude response of subcarrier i, $|\mathrm{H}_i|$ given in (3), is also periodic. In most cases, the CSI amplitude can effectively capture the dynamics of the respiration signal. However, at some specific locations, when the phase difference between the static component H_i^s and the dynamic component H_i^d is nearly zero, the variations of the CSI amplitude will be small, leading to high monitoring errors.

This is illustrated in Fig 1, where the geometric relationship of the static and dynamic components is presented. The dynamic components are $\overrightarrow{SD}_i$, $i = 1, 2, 3, 4$, and the static component is $\overrightarrow{OS}$. We can see that when the dynamic vector oscillates between $\overrightarrow{SD}_1$ and $\overrightarrow{SD}_2$, the CSI amplitude varies between $|\overrightarrow{OD}_1|$ and $|\overrightarrow{OD}_2|$, with very small variations. Such small variations in the CSI amplitude leads to a very weak respiration signal and thus high detection error if used alone.

On the other hand, consider the phase response of subcarrier i, $\angle \mathrm{H}_i$, which can be derived as [15], [16]

$$\angle \mathrm{H}_i = \angle \mathrm{H}_i^s - \arctan\left\{ \frac{|\mathrm{H}_i^d| \sin(\angle \mathrm{H}_i^s - \angle \mathrm{H}_i^d)}{|\mathrm{H}_i^d| \cos(\angle \mathrm{H}_i^s - \angle \mathrm{H}_i^d) + |\mathrm{H}_i^s|} \right\}. \tag{5}$$

Similarly, the phase response of subcarrier i is also periodic, which can also be used to detect the respiration rate. However, there are also some cases where the phase information is not effective for measuring respiration signals. As shown in Fig. 1, when the dynamic vector oscillates between $\overrightarrow{SD}_3$ and $\overrightarrow{SD}_4$, the phase value changes only slightly between $\angle\overrightarrow{OD}_3$ and $\angle\overrightarrow{OD}_4$. Such negligible variations in phase value makes it hard to detect the respiration rate with phase information alone in this situation.

Fortunately, we can see that in the first example, when the variation in CSI amplitude is small, the variation in CSI phase is between $\angle\overrightarrow{OD}_1$ and $\angle\overrightarrow{OD}_2$, which is quite large. On the other hand, in the second example when the variation in CSI phase is small, the change in CSI amplitude is between $|\overrightarrow{OD}_3|$ and $|\overrightarrow{OD}_4|$, which is also quite large. Thus these two types of CSI data are complementary to each other. This observation motivates us to leverage bimodal CSI data, including CSI amplitude and phase, for resilient respiration rate monitoring.

C. Phase Difference

CSI phase data is indicative of the phase shift caused by the wireless channel, but the measured CSI phase for each antenna is not usable, due to the randomness introduced in the RF chain, such as packet boundary detection (PBD), the sampling frequency offset (SFO), and central frequency offset (CFO) [15], [17]. To avoid the large noise caused by the randomness in the transmission process, we use the measured *phase difference* data instead in ResBeat, which is the difference between the phase readings from two neighboring antennas of the 802.11n NIC for the same received WiFi packet, given by

$$\Delta\angle\widehat{H}_i = \Delta\angle \mathrm{H}_i + \Delta\phi + \Delta\mathcal{N}, \tag{6}$$

where $\Delta\angle \mathrm{H}_i$ is the true phase difference of subcarrier i, $\Delta\phi$ is an unknown difference in phase offsets, which is a constant [21], and $\Delta\mathcal{N}$ is the noise difference between the two antennas.

It has been proved in our previous work that using phase difference data, the randomness introduced by PBD, SFO, and CFO can be effectively mitigated, since both antennas are on the same NIC and are affected by the same sources for these random terms [15], [16]. Obviously, $\Delta\angle\widehat{H}_i$ is a relatively more stable signal with respect to different received packets, since the randomness due to PBD, SFO, and CFO are canceled. The mean of the estimated phase difference is different from the true phase difference by a constant term $\Delta\phi$, and its variance is only twice of the noise variance [15], [16].

D. Experimental Validation

We verify the observations obtained by the model and analysis with experiments. In these experiments, three antennas are used for receiving data, and each antenna can collect CSI amplitude and phase from 30 subcarriers. Thus, we can obtain 90 amplitude readings and 90 phase readings in total for each received packet. We then compute 30 phase difference values between the phase readings from antenna 1 and antenna 2, another set of 30 phase difference values between antenna 2 and antenna 3, and a third set of 30 phase difference values between antenna 3 and antenna 1. The experiment is repeated twice, while each time the relative position of the patient and the WiFi antennas is different. And 100 WiFi packets are transmitted and received each time. The collected amplitudes

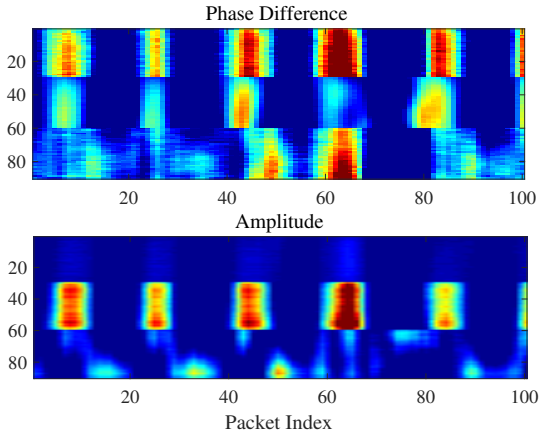

Fig. 2. Colormap for the captured CSI phase differences and amplitudes for experiment 1.

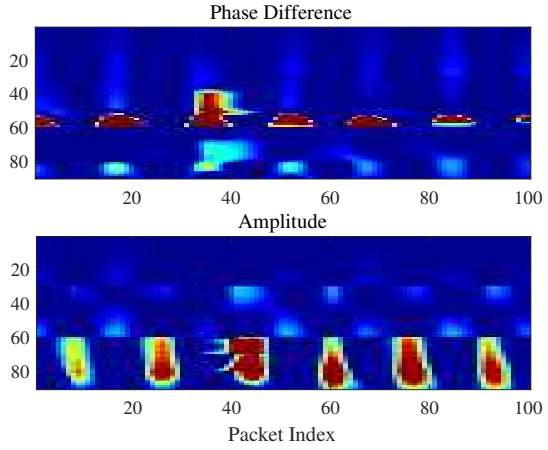

Fig. 3. Colormap for the captured CSI phase differences and amplitudes for experiment 2 (when the patient-antenna position is changed).

and phase differences are plotted in Fig. 2 and Fig. 3 for the two experiments, respectively. In both figures, the upper plot presents the collected phase differences, while the lower plot is for the collected amplitudes. The x-axis is for the 100 received packets, while the y-axis is for the 90 values obtained for each packet (i.e., antenna 1 to 3, and 30 subcarriers on each antenna). Different colors indicate different signal strengths: more red means the signal is stronger, while more blue means the signal is weaker.

The colormaps in Fig. 2 and Fig. 3 all exhibit certain strong-weak periodic pattern for the signal strength in the packet index direction. Obviously, the periodic pattern represents the respiration signal, and we are actually sampling the chest movement (or, respiration) using the 100 packets.

As can be seen in the upper plot in Fig. 2, the phase differences between antennas 1 and 2 capture a strong periodic respiration signal. However, when the relative position of the patient and the antennas are changed, the phase differences from the same pair of antennas only capture a very weak respiration signal (with very small change in strength over the 100 packets), as shown in the upper plot in Fig. 3. Similar observation can be made for the amplitudes from antenna 2 in the lower plot in Fig. 2, and that from the same antenna 2 in the lower plot in Fig. 3. To better monitor human respiration, it helps to leverage the amplitudes from antenna 3, and the phase differences between antennas 2 and 3, as shown in Fig. 3, when the patient-antenna position is changed.

III. The ResBeat System Design

A. System Architecture

The main idea of the proposed ResBeat system is to sample the human respiration signal with chest-reflected WiFi packets, and detect the respiration signal from realtime bimodal CSI data extracted from 5GHz WiFi devices. The ResBeat system can effectively exploit realtime bimodal CSI data to estimate the respiration rate due to three reasons. First, CSI amplitude and phase difference data are quite stable over consecutive packets in a stationary environment, both of which can effectively capture the human breathing signal. Second, CSI amplitude and phase difference data are complementary to each other with respect to their resilience to the two anomalous cases as shown in Fig. 1. Using the bimodal data can effectively deal with anomalous breathing signals. Third, ResBeat is robust to environment interference and body movements by using the bimodal CSI data. We propose an adaptive signal selection method to select the most sensitive CSI data, i.e., amplitude or phase difference, to mitigate the effect of anomalous breathing signals.

Fig. 4 presents the ResBeat system architecture, which consists of three main modules: (i) Data Preprocessing, (ii) Adaptive Signal Selection, and (iii) Breathing Signal Monitoring. The Data Preprocessing module includes CSI data extraction and data calibration. For CSI data extraction, we obtain 90 CSI amplitude values and 90 phase difference values from the three WiFi antennas for each received packet from the modified Intel 5300 NIC device driver. For data calibration, we employ the EWMA method to obtain the *environment component*, while the *breathing component* can be extracted by subtracting the environment component from the denoised CSI data. The Adaptive Signal Selection module includes signal energy detection, movement detection, and signal selection. We use the normalized breathing component to compute the energy of the data (for either CSI amplitude or phase difference data from 30 subcarriers). We then implement a counting method for three CSI phase difference groups for detection of body movements. Moreover, we develop a signal selection algorithm to boost the reliability of bimodal CSI data for breathing signal monitoring by selecting the most sensitive signal group from CSI amplitude and phase difference data groups. In the Breathing Signal Monitoring module, peak detection is employed to derive the respiration rate from the realtime CSI data.

B. Data Preprocessing

1) CSI Data Extraction: We collect 90 CSI values (i.e., 90 CSI amplitude and 90 phase values) for every received packet from the three antennas of the IEEE 802.11n NIC, each of which provide CSI values from 30 subcarriers. We then compute the CSI phase difference values between antennas 1 and 2, antennas 2 and 3, and antennas 3 and 1, respectively, as

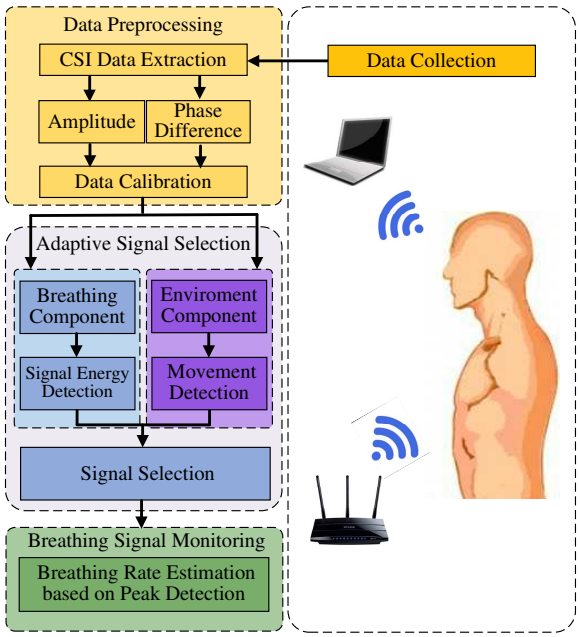

Fig. 4. The ResBeat system architecture.

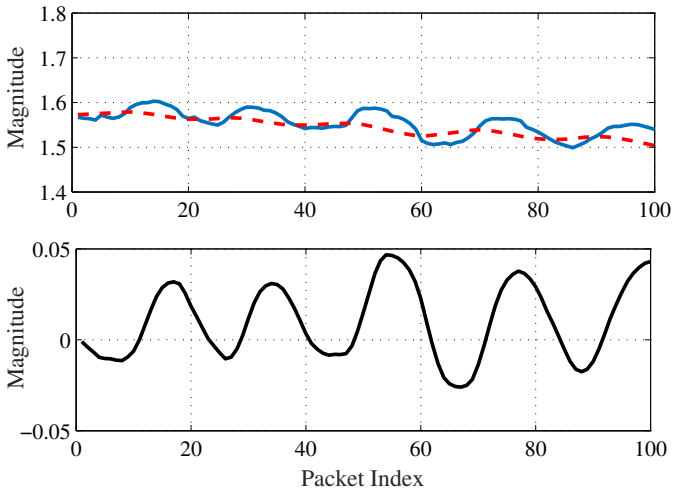

Fig. 5. Data calibration results.

in (6). The data collected from a sequence of WiFi transmissions are organized into three CSI amplitude groups (one for each antenna) and three CSI phase difference groups (one for each antenna pair), to be processed in the following modules.

2) Data Calibration: Data calibration is to identify the static component (or, the *environment component*) and the dynamic component (or, the *breathing component*) from the original CSI amplitude and phase difference data. The environment component represents the features of wireless channel from the surrounding environment such as reflection from walls, desks and stationary body of a person. On the other hand, the breathing component represents the change of wireless signal due to chest movements when inhaling and exhaling.

In ResBeat, the environment component is obtained using the EWMA method, which is based on a first-order autoregressive model [22]. Let $X(t)$ be the realtime CSI data (i.e., CSI amplitude or phase difference), and $\bar{X}(t)$ be its local mean. Then $\bar{X}(t)$ can be updated as

$$\bar{X}(t) = \alpha \cdot X(t) + (1-\alpha) \cdot \bar{X}(t-1), \text{ for } t = 1, ..., n, \quad (7)$$

where α is a parameter that determines the relative weights of the present sample and historical values, and n is the total number of observed samples. In our experiments, we set $\alpha = 0.1$ to obtain the local mean, which provides an estimate for the environment component.

We utilize the EWMA method for extracting the environment component for three reasons. First, the EWMA method does not require a large data buffer and is thus suitable for realtime breathing monitoring. Second, as the moving average (MA) method, the EWMA method can effectively extract the trend of the realtime data, and the breathing signal can be obtained by removing this trend. Last but not least, compared with MA, EWMA is more sensitive to the more recent sample data. When the body moves, EWMA will capture a large change in M_t and thus can have a more rapid response, which is beneficial for detecting environmental changes.

After obtaining the environment component, we first apply the MA method to the original CSI data to remove high frequency noises, with a window size set to 3. Then, the breathing component can be extracted by subtracting the environment component from the denoised CSI data. Fig. 5 illustrates the calibration of the original phase difference data for subcarrier 5 between antennas 1 and 2. We can see in the top plot that the original phase difference values have a direct current (DC) component as well as high frequency noises. Applying the EWMA method, we can obtain the environment component (dashed line), which is the trend of the original phase difference. Then, the breathing component can be extracted by de-noising the CSI phase difference data and removing the environment component, which exhibits a sinusoidal-like periodicity over the received packets as shown in the bottom plot in Fig. 5.

C. Adaptive Signal Selection

In the adaptive signal selection module, signal energy detection and movement detection are implemented to select the most sensitive signal group from the three CSI amplitude groups (one from each antenna) and three CSI phase difference groups (one from each antenna pair), since some signal group is more sensitive to human breathing for a given testing environment.

1) Movement Detection: Since the collected CSI is also affected by large body movements and the mobility in the surroundings, such as people walking nearby, the influence of such large noises should be firstly addressed before respiration monitoring. Since the surrounding movements is usually much larger than that of human breathing, it would be very challenging to separate the respiration signal from the strong noises. Thus, we design a movement detection module to firstly detect if the environment is suitable for human respiration rate monitoring.

In this module, phase difference data is leveraged to compute the environment component, because it has a fixed range between $-\pi$ and π, unlike CSI amplitude data that has a

relatively wider variable range. We calculate the environment components with EWMA for all the phase difference data over the 30 subcarriers, and then compare it with the adjacent average values. A body movement is regarded to be detected if the current average value is lower than 95% or larger than 105% of the previous average value. Although the different environmental setup could lead to different environment component variations for the same body movement, these two parameters are not required to be calibrated for a different setup. This is because the parameters we used in the algorithm is to determine if the body movement considerably changes the wireless channel feature. No matter what environment settings or body movements are applied, the system is required to re-select the signal once a significant environment component variation is detected.

Through experiments, we find that small movements of the patient body (e.g., slight hand move) may also generate changes in the environment component, but these changes are acceptable for breathing signal extraction. Since the EWMA algorithm detects the variation trend of the signal, the body movement will not generate sharp peaks in the environment component. Instead, a large body movement generates continuous increase or decrease, while the variation caused by small body movement do not last for long. To mitigate the influence of small body movements, we propose a *counting method* to ensure that only large body movements will be detected by the algorithm.

The counting method is presented in Algorithm 1 with the following steps. First, the counter is initialized to 0. Then, the counter will be increased by 1 when the current average value of phase difference data is lower than 95% or larger than 105% of the last average value. From our experiments, we found that the interference of small body movements could be mitigated by setting the time threshold to 1 second. Thus, a large body movement is regarded to be detected if and only if the counter reaches 10, since the sampling rate is 10 Hz in the prototype system. However, if the average falls back to the range of 95% to 105% of the previous average, before the counter reaches 10, the counter will be reset to 0.

In ResBeat, we implement the counting method that uses the three CSI phase difference data groups for movement detection. Since the chest fluctuation caused by respiration is much weaker than other body movements (e.g., while walking), breath monitoring for a randomly moving user is challenging. Furthermore, due to the multipath effect, other moving objects around the patient will also generate considerable interference in sampled CSI data. If such a movement is detected, ResBeat will wait for 2 seconds to see whether the environment quiets down and is suitable for breathing monitoring. This is because, detecting a very weak signal from strong noise is a challenging and maybe intractable problem; it may require highly complex signal processing techniques, and may not be suitable for a realtime system. Thus, to provide robust breath monitoring, the system is designed to select the most sensitive signal once the environment quiets down. The signal selection algorithm given in Algorithm 2 is only executed when the movement detection algorithm detects no movement.

Algorithm 1: Movement Detection Algorithm

Input: current average of the environment components of all phase differences (denoted by A_n), and the averages in the two previous states (i.e., A_{n-1} and A_{n-2}) ;
Output: $move\_flag$;
//Initialization ;
Set $move\_flag = 0$;
Set $counter = 0$;
//Movement detection ;
if $counter < 9$ **then**
  if *(($A_n > 1.05A_{n-1}$) and ($A_{n-1} > 1.05A_{n-2}$)) or (($A_n < 0.95A_{n-1}$) and ($A_{n-1} < 0.95A_{n-2}$))* **then**
    $counter++$;
  end
  else
    $counter = 0$;
  end
end
else
  Set $move\_flag = 1$;
  Set $counter = 0$;
  Return $move\_flag$;
end

2) Signal Energy Detection: For adaptive signal detection, we evaluate the energy level of the breathing components, as an indicator of the sensitivity of CSI amplitude and phase difference data group. Recall that each CSI data group includes 30 samples for each received packet. We use a time window with a size of 20 packets to compute the local energy of CSI data group j at time t, denoted by $E_j(t)$, given by

$$E_j(t) = \sum_{k=t-19}^{t} \sum_{i=1}^{30} \left| Y_{ij}^d(k) \right|^2, \tag{8}$$

where $Y_{ij}^d(k)$ is the normalized breathing component data for subcarrier i in CSI data group j at time k. Since the system will wait for 2 s once movement is detected, 2 s of data has already been sampled by now before the selection algorithm. To make full use of the sampled data, we set the window size to 2 s, which translate to 20 samples since the sampling frequency is 10 Hz. Compared with other advanced approaches such as an FFT based method, the signal energy detection method can exploit smaller amount of samples to measure the sensitivity of CSI amplitude and phase difference data, which help to satisfy the requirement of realtime processing.

3) Signal Selection: This module is to select the most sensitive group from the six CSI data groups, for accurate breathing rate measurement. The procedure is presented in Algorithm 2. The input parameters include the movement detection flag, mov_flag, and the local energy of each signal group, E_1, E_2, ..., E_6, computed as in (8). The output is the index of the most sensitive CSI data group.

In the beginning, we use 30 phase difference data from antennas 1 and 2 to implement the signal selection no matter whether a movement is detected or not. After initialization, we use the movement detection module to determine whether the environment or the patient has a large move. When a movement is detected, we run the signal selection algorithm

Algorithm 2: Signal Selection Algorithm

Input: movement detection flag (mov_flag) and the local energy of each data group (E_1, E_2, ..., E_6) ;
Output: index of the most sensitive data group ;
Set $initialize\_flag = 1$;
Set $select\_num = 1$;
if $mov\_flag == 1$ **then**
  Wait for 2 seconds ;
  Set $mov\_flag = 0$;
  Set $select\_count = 0$;
  while *(*$(mov\_flag == 0)$ *or (*$initialize\_flag == 1$*))* **do**
    Sort the data groups (1, 2, ..., 6) in descending order of their local energies (E_1, E_2, ..., E_6) ;
    if *(The new index of the first group equals to the former index of the first group)* **then**
      $select\_count++$;
      if $select\_count == 3$ **then**
        Set $select\_num$ to the index of Group 1 ;
        Set $initialize\_flag = 0$;
        Set $select\_count = 0$;
        Break ;
      end
    end
    else
      Set $select\_count = 0$;
    end
  end
end
Return $select\_num$;

again. First, the system will wait for 2 seconds, so that the environment components obtained by EWMA can return to stable values (i.e., to recover from the movement). Then, the system sorts the signal groups (i.e., 1–6) in descending order of their local energy levels (i.e., E_1, E_2, ..., E_6). If a group is ranked top 1 for three consecutive times, it will be selected as the most sensitive data group. If the top-ranked group becomes a different group before $select\_count$ reaches 3, the counting number will be reset to zero. Moreover, if a new movement is detected, the signal selection algorithm will be restarted.

ResBeat keeps on using the previously selected data group to measure and monitor respiration rate, until the next most sensitive data group is selected. Then the new signal group will be used instead. The proposed signal selection algorithm is robust to environment interference and small movements of the patient body. Moreover, with the signal selection module, ResBeat can rapidly recover from the patient's large body movements.

D. Breathing Signal Monitoring

Although both CSI amplitude and phase difference data can capture breathing induced small movements (i.e., inhaling and exhaling), using the most sensitive signal group helps to effectively mitigate the effect of anomalous breathing signals in some corner cases. Traditionally, FFT based method can estimate the breathing frequency using a large-sized sliding window with good accuracy. However, an FFT based approach does not work well for realtime estimation of respiration rates, due to the use of the large time window.

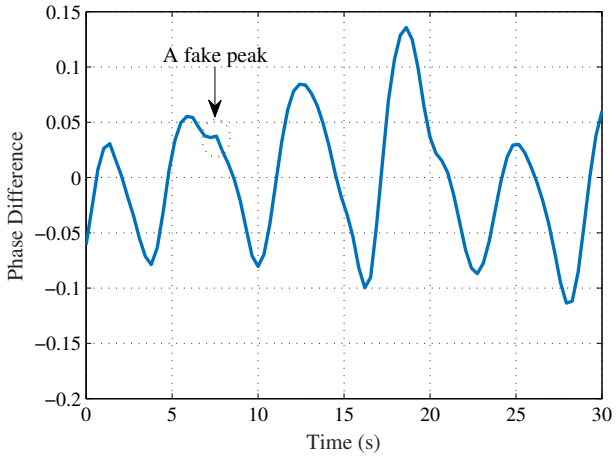

Fig. 6. Calibrated breathing signal that has a fake peak.

The proposed ResBeat system utilizes peak detection instead to compute the respiration rate in realtime, using the selected, most sensitive signal group. However, the breathing components can still have some fake peaks, which is not a true peak but its value is larger than its two neighboring samples (on both sides). These fake peaks could be caused by small body movements or heartbeats of the user. Fig. 6 shows the calibrated breathing signal for a period of 30 s, which contains five breathing cycles. It can be seen that there is a fake peak located in the second breathing cycle.

Even though the phase difference of the fake peak is higher than its two adjacent samples on both sides, it should not be considered as a peak of the breathing signal. A sliding window based method is applied to mitigate the influence of such fake peaks. After observing numerous fake peaks, we found that although the fake peak is larger than its two adjacent samples, the length of the fake peaks are no longer than 0.5s, which means 5 samples for the 10 Hz sampling frequency. Thus, to distinguish fake peaks from real peaks, the window size should be larger than 5 samples. Consequently, we set the window size to 7 samples to find all the true peaks in a buffer of 100 samples. The algorithm checks whether the sample at the center of the window is the maximum among all the samples in the small window.

Once the fake peaks are detected and ignored, we can compute the period of the breathing signal by averaging all peak-to-peak intervals. Because the buffered data is updated in realtime, we use another small buffer with size 20 to store the most recent 20 estimated breathing periods $t_i, i = 1, 2, ..., 20$. Then, the estimated period of the breathing signal is computed as $\mathcal{T} = \frac{1}{20}\sum_{i=1}^{i=20} t_i$, and the estimated respiration rate in bpm (breaths per minute) is computed as

$$\mathcal{R} = 60/\mathcal{T}. \tag{9}$$

IV. Experimental Study

A. Experiment Configuration

The ResBeat system is implemented on a Ubuntu Desktop 14.04 LTS OS for both the transmitter and receiver, each equipped with an Intel 5300 NIC operating in the 5GHz

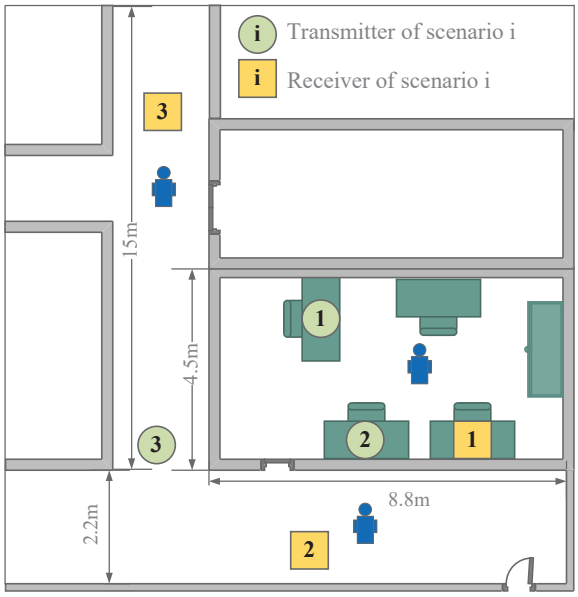

Fig. 7. Configuration of the experiments to validate the ResBeat performance.

ISM band. The transmitter is a Lenovo laptop set in the injection model, which transmits 10 packets per second using one antenna. The receiver is an Acer laptop working in the monitoring mode for collecting CSI data. The three antennas of the WiFi NIC at the receiver are placed in a row at an interval of 2.68 cm (i.e., half of the wavelength). The delay caused by the different distances from two adjacent receiver antenna to the transmitter antenna is lower than 9 ns, which can be ignored for respiration monitoring. Therefore, packet can be considered as being received by different antennas simultaneously. The ResBeat system collects realtime CSI amplitude and phase difference data from the three antennas from each received packet.

We test the Resbeat system in three different environments as shown in Fig. 7. In the first environment, both the transmitter and the receiver are placed in a computer Lab of size 4.5 $\times$ 8.8 m^2, while the patient is in the same room. The second test is carried out with the through-wall scenario to test the performance of ResBeat under weak WiFi signals. The third test is carried out in an empty corridor to validate the impact of longer distance between the transmitter and the receiver. Omnidirectional antennas are used for the transmitter and the receiver in all three scenarios. In addition, the NEULOG Respiration sensor is used to measure the ground truth of the patient's breathing rate [23]. NEOLOG respiration sensor utilized in our experiments is a belt sensor. It could be tightly bound on the human chest, so the monitor can accurately monitor the chest motion caused by inhaling or exhaling with 15 bits ADC resolution and 100 sampling frequency [23]. Unfortunately, the estimated respiration rate is not directly provided by its user interface. Thus, in order to conduct a straightforward comparison of the respiration rate between our system and the NEULOG sensor, We leverage the same breathing rate estimation algorithm, as introduced in Section III-D, to calculate the respiration rate from the NEULOG recorded respiration signal as the ground truth.

Three receiving antennas are equipped on the receiver in the experiments. This is because, our system is currently composed of one transmitter and one receiver, and the maximum number of antennas supported by the Intel 5300 NIC is 3. Moreover, the phase difference data used in the system is calculated between two receiving antennas. Therefore, at least 3 receiving antennas is required if we want to apply adaptive signal selection to the multiple phase difference signals. Using the off-the-shelf Intel 5300 NIC does not allow us to evaluate the impact of more receiving antennas

As discussed in Section II-B, the breathing signal could be extremely weak at certain measurement locations, which is hard to detect [18]. To measure the resilience of breathing rate measurement methods, we define a *success rate* performance metric, denoted by η, as

$$\eta = \frac{1}{N}\sum_{i=1}^{N}\left(\frac{\text{sign}(2-e_i)+1}{2}\right), \tag{10}$$

where e_i is the breathing estimation error in bpm for measurement location i, sign$(\cdot)$ is the `sign` function that returns 1 or -1, and N is the total number of different locations where respiration rate is measured. The success rate represents the ratio of the number of locations that have an error less than 2 bpm to the total number of locations.

B. Performance of Breathing Rate Estimation

Fig. 8 plots the cumulative distribution functions (CDF) of estimation errors of breathing rate estimation in the computer laboratory, through-wall, and long corridor scenarios. We find that ResBeat achieves quite accurate estimations in all the three scenarios. The maximum error is 1.75 bpm, which occurs in the most challenging through-wall scenario. The median errors are 0.25 bpm, 0.25 bpm, and 0.29 bpm for the computer laboratory, long corridor, and through-wall cases, respectively. The breathing estimation errors in the laboratory and long corridor scenarios are lower than that in the through-wall scenario. This is because the breathing signal in the through-wall scenario is much more attenuated by the wall. In fact, the accuracy for the through-wall scenario is still sufficiently high. We conclude that the proposed ResBeat system is accurate in all the three scenarios.

Fig. 9 presents the success rates, as defined in (10), for ResBeat and two benchmark schemes in the computer laboratory, through-wall, and long corridor scenarios. In this experiment, we use an amplitude based method [14] and PhaseBeat [15], [16] as benchmarks for success rate comparison. We find that the proposed ResBeat system achieves high success rates of 91.54% and 93.04% in the laboratory and long corridor case, respectively, and of 86.51% in the through-wall scenario. These results indicates that a stronger breathing signal can help to achieve higher estimation accuracy. The success rate of ResBeat is higher than that of the other two benchmark schemes in all the three environments. This is because ResBeat exploits bimodal CSI data and the adaptive signal selection method to select the most sensitive data group. Thus it can effectively mitigate the effect of anomalous breathing signals at some bad locations.

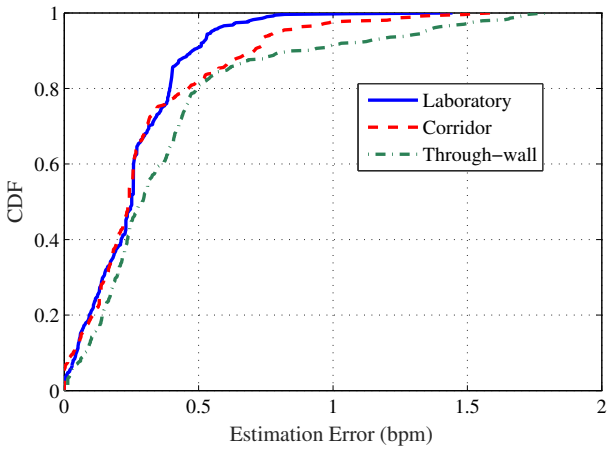

Fig. 8. Performance of breathing rate estimation (i.e., CDFs of estimation errors) in the computer lab, long corridor, and through-wall scenarios.

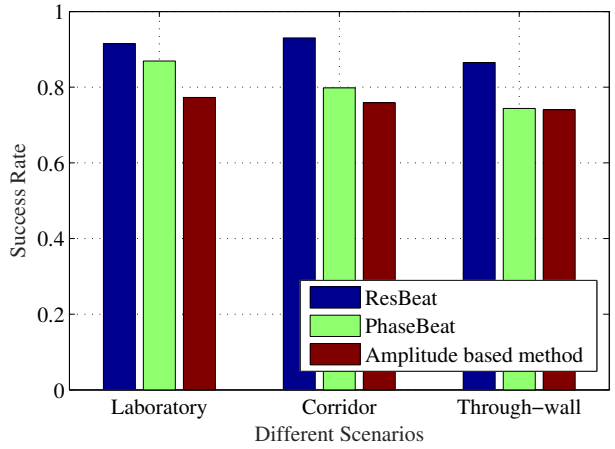

Fig. 9. Success rates of ResBeat and two benchmark schemes (Amplitude based and PhaseBeat) in the computer laboratory, through-wall, and long corridor scenarios.

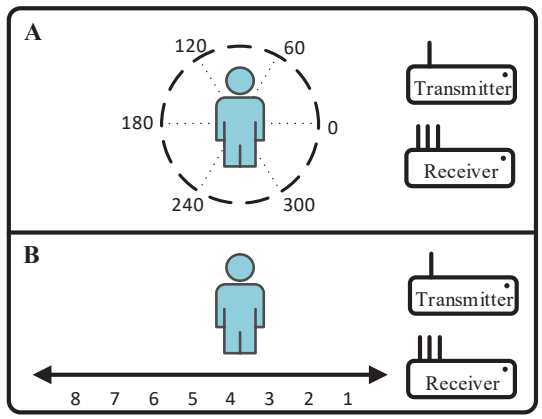

Fig. 10. Illustrate the different orientations and distances between the patient and WiFi devices.

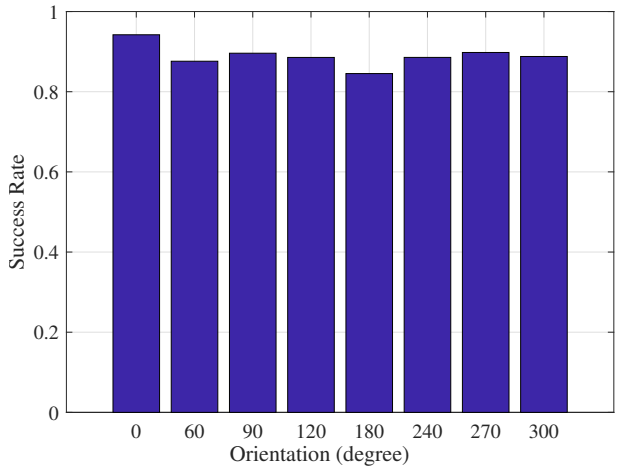

Fig. 11. Success rates for different orientations of the patient's body.

C. Impact of Environments and System Parameters

In this section, we evaluate the impact of the test environment and the system parameter on the performance of ResBeat. We first examine the effect of different orientations of the patient body and different patient-WiFi distances in the laboratory environment. As shown in Fig. 10, the WiFi transmitter and receiver are put side by side on a table at one end of the room. In the upper plot, the patient body can have different orientations: a 0° orientation means the patient is directly facing the WiFi devices, while a 180° orientation means the patient is facing the opposite direction. Intuitively, the 0° orientation can better reflect WiFi signals and generate a larger variation in the distance that the reflected signal travels, than the 90° or 270° orientations. In the lower plot in Fig. 10, the patient is always facing the WiFi devices, but the distance in between is varied, which can lead to various strengths of the reflected signal.

Fig. 11 It shows that when the patient directly faces the devices, the success rate achieves the maximum value, which is 94.21%. When the user does not face the WiFi devices, the success rate is still very high, such as 87.61% and 89.79% for 90 and 270 degrees, respectively. This is because the system can automatically find the most sensitive signal for respiration monitoring. The lowest success is 87.63%, which is obtained when the patient is facing the opposite direction from the WiFi devices. The result shows that the reflected signal strength is the highest when the patient directly faces the WiFi devices. As the user turns around, it becomes harder for the RF signal to hit on and be reflected directly from the chest. Although the signal can still reach the chest by reflecting first from the surroundings (e.g., walls and ceiling), the strength of the signal becomes weaker, and thus the lower success rates.

Fig. 12 presents the success rates for different distances between the patient and the WiFi devices, as shown in the lower plot in Fig. 10. When the distance is increased, the success rate of ResBeat is degraded because of the loss of reflected signal strength. Moreover, the success rate is higher than 91.34% when the distance is from 1 m to 3 m, but drops significantly as the distance is over 4 m. This is because when the patient is not so far away, most of the reflected signals from surroundings can reach the chest. These signals can also help to increase the strength of the chest-reflected signal. When the patient is too far away, fewer WiFi signals can be reflected by the chest. Thus, the success rate of ResBeat decreases

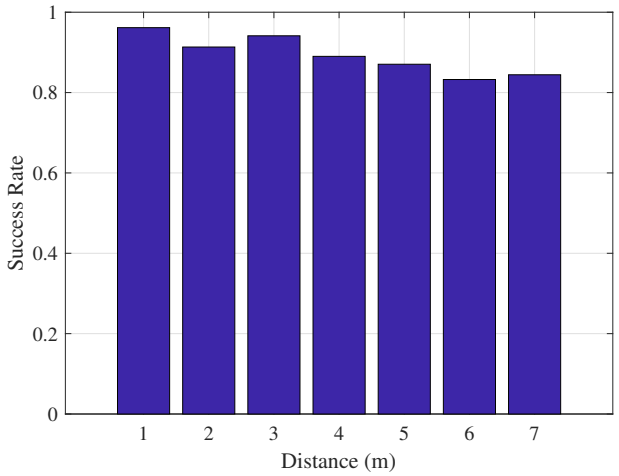

Fig. 12. Success rates for different distances between the patient and the WiFi devices, while the patient is directly facing the WiFi devices.

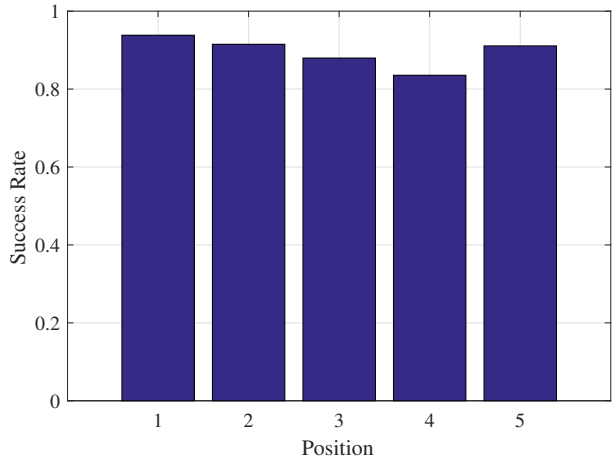

Fig. 13. Success rates for different positions in the laboratory.

significantly for longer distances.

To examine the robustness of ResBeat, we evaluate it when the patient, the transmitter, and the receiver are randomly put at five different set of positions in the lab. The success rate for the five positions are given in Fig. 13. We find that the minimum success rate is obtained in position 4, which is 83.55%, while the highest success rate is achieved in position 1, which is 93.83%. Fig. 13 shows that success rates for all the five different positions are all higher than 83.55%, and three of them are higher than 91.09%. The results demonstrate that ResBeat is quite robust for monitoring human breathing rate in different environments.

We also examine the impact of the EWMA parameter α (see (7)) on the ResBeat success rate. From (7), if α is too small, EWMA will hardly capture the instant change of human body in realtime. However, if α is too large, the EWMA result will be too sensitive to the instant movement, making it hard to extract the environment component. To identify the proper α value, we obtain the success rates for different α, which are presented in Fig. 14. We find the success rate achieves the maximum when α is set to 0.1. The success rate decreases

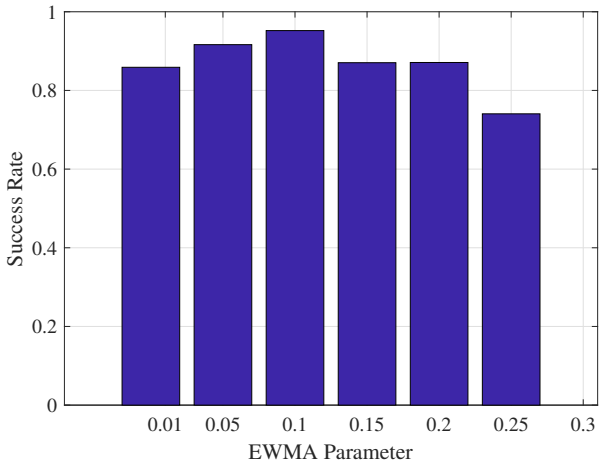

Fig. 14. Success rates for different EWMA parameter α.

significantly when α is smaller than 0.05 or larger than 0.25. Consequently, we set $\alpha = 0.1$ in the EWMA algorithm.

V. Related Work

This work is closely related to RF signal based vital sign monitoring and CSI based RF sensing. We briefly review these two classes of related work in the following.

Several RF sensing based systems have been proposed in the literature for vital sign monitoring. For these systems, WiFi, Radar, and radio-frequency identification (RFID) techniques play an important role. For example, UbiBreathe is a representative WiFi based system for monitoring human breathing rate [11]. It leverages RSS of WiFi signals to estimate the respiration rate, but the patient should remain in the line-of-sight path of the two RF devices. Alternatively, mmVital utilizes the RSS of 60 GHz millimeter wave (mmWave) signals [8].

For better performance, CSI based methods are proposed by using amplitude and phase difference data. The first work is to use CSI amplitude for measuring breathing and heart rates when the patient is sleeping [14]. Our recent works, i.e., PhaseBeat [15], [16] and TensorBeat [17], employ CSI phase difference data to estimate a single or multiple persons' breathing signals, respectively. The latter is achieved by increasing the dimension of CSI data and apply tensor decomposition to separate the individual breathing signals. In addition, the CSI-ratio based technique is proposed recently to track human respiration in the indoor environment [24]–[26]. Different from the direct implementation of the amplitude or phase data of CSI, the CSI-ratio is more robust to the interference due to changes in the environment. However, these works may not be effective for weak breathing signals in some corner cases [18], and may suffer low success rates in some adverse environments. The focus in this work is to use bi-modal CSI data to improve the robustness over such adverse environments.

Among Radar based techniques, the FMCW radar can extract breathing signals from multiple patients, as well as detecting the heart beats signal [7]. There are some other

vital sign monitoring systems based on the Radar technique, including ultra-wideband (UWB) Radar [10] and Doppler Radar [9]. However, such Radar techniques all require some special hardware that incurs higher cost.

Moreover, there have been new interest in exploit the low-cost passive RFID tags for vital sign monitoring [27]–[29]. In an interesting recent work TagBreathe [27], RFID tags are attached to a patient's clothes. When interrogated by a reader, the tags will generate backscatter radio waves, which carries the breathing signal since the tags moves with the patient chest. The phase value of the RFID responses are evaluated to extract the breathing signal. In our recent work AutoTag [28], [29], we also use multiple tags attached to the patient body to sample the breathing signal. A novel technique is developed to mitigate the frequency hopping offset for FCC-compliant RFID systems, to enable many realtime applications including vital sign monitoring. We also develop a unsupervised deep learning based on recurrent variational autoencoder for detection of sleep anomaly such as apnea detection, which is highly accurate and does not require labeled medical training data.

In addition, CSI based RF sensing have been widely applied to activity recognition, person identification and counting, and anomaly detection. For CSI based activity recognition, the E-eyes system can recognize household activities such as talking a shower and walking using CSI amplitude [30], where multiple-dimensional dynamic time warping (MD-DTW) and earth movers distance (EMD) techniques are used for walking activity tracking and in-place activity identification, respectively. The WiHear system can recognize spoken words from lip movement by measuring CSI changes, where specialized directional antennas are used to enhance the received power [31]. The CARM system provides a fundamental model for CSI data dynamics for a given human activity [20]. Moreover, CSI values are used for recognizing gestures [32], [33] and keystrokes [34].

For CSI based person identification and counting, the Wi-Who system is the first to use CSI amplitude for person identification based on gait analysis [35]. The

Grey Verhulst Model is used for crowd counting using CSI values [36]. Moreover, deep learning has been used to improve the performance for user authentication [37] and person counting [38]. CSI based anomaly detection includes movement detection [39], fall detection [40], fire detection [41], temperature measurement [42], and moisture detection [43], [44]. CSI based indoor localization techniques mainly focus on deep learning enhanced fingerprinting [45]–[47] and angle of arrival (AOA) based methods [48].

VI. Conclusions

In this paper, we proposed the ResBeat system for resilient respiration rate monitoring with commodity WiFi. We developed the ResBeat system including data preprocessing, adaptive signal selection, and breathing signal monitoring, where bimodal CSI data were shown to be complementary to each other were exploited to achieve high resilience. The superior performance of ResBeat was validated with extensive experiments under three different scenarios.

References

[1] X. Wang, C. Yang, and S. Mao, "ResBeat: Resilient breathing beats monitoring with realtime bimodal CSI data," in *Proc. IEEE GLOBECOM 2017*, Singapore, Dec. 2017, pp. 1–6.

[2] O. Boric-Lubeke and V. Lubecke, "Wireless house calls: Using communications technology for health care and monitoring," *IEEE Microwave Mag.*, vol. 3, no. 3, pp. 43–48, Apr. 2002.

[3] C. Hunt and F. Hauck, "Sudden infant death syndrome," *Can. Med. Assoc. J*, vol. 174, no. 13, pp. 1309–1310, Apr. 2006.

[4] M. L. R. Mogue and B. Rantala, "Capnometers," *Journal of clinical monitoring*, vol. 4, no. 2, pp. 115–121, Apr. 1988.

[5] X. Wang, R. Huang, and S. Mao, "SonarBeat: Sonar phase for breathing beat monitoring with smartphones," in *Proc. ICCCN 2017*, Vancouver, Canada, July/Aug. 2017, pp. 1–8.

[6] X. Wang, R. Huang, and S. Mao, "Demo abstract: Sonarbeat: Sonar phase for breathing beat monitoring with smartphones," in *Proc. IEEE SECON 2017*, San Diego, CA, June 2017, pp. 1–2.

[7] F. Adib, H. Mao, Z. Kabelac, D. Katabi, and R. Miller, "Smart homes that monitor breathing and heart rate," in *Proc. ACM CHI'15*, Seoul, Korea, April 2015, pp. 837–846.

[8] Z. Yang, P. Pathak, Y. Zeng, X. Liran, and P. Mohapatra, "Monitoring vital signs using millimeter wave," in *Proc. IEEE MobiHoc'16*, Paderborn, Germany, July 2016, pp. 211–220.

[9] P. Nguyen, X. Zhang, A. Halbower, and T. Vu, "Continuous and fine-grained breathing volume monitoring from afar using wireless signals," in *Proc. IEEE INFOCOM'16*, San Francisco, CA, Apr. 2016, pp. 1–9.

[10] J. Salmi and A. F. Molisch, "Propagation parameter estimation, modeling and measurements for ultrawideband mimo radar," *IEEE Trans. Microw. Theory Technol.*, vol. 59, no. 11, pp. 4257–4267, Nov. 2011.

[11] H. Abdelnasser, K. A. Harras, and M. Youssef, "Ubibreathe: A ubiquitous non-invasive wifi-based breathing estimator," in *Proc. IEEE MobiHoc'15*, Hangzhou, China, June 2015, pp. 277–286.

[12] D. Halperin., W. J. Hu., A. Sheth., and D. Wetherall., "Predictable 802.11 packet delivery from wireless channel measurements," in *Proc. ACM SIGCOMM'10*, New Delhi, India, Sept. 2010, pp. 159–170.

[13] Y. Xie, Z. Li, and M. Li, "Precise power delay profiling with commodity WiFi," in *Proc. ACM Mobicom'15*, Paris, France, Sept. 2015, pp. 53–64.

[14] J. Liu, Y. Wang, Y. Chen, J. Yang, X. Chen, and J. Cheng, "Tracking vital signs during sleep leveraging off-the-shelf WiFi," in *Proc. ACM Mobihoc'15*, Hangzhou, China, June 2015, pp. 267–276.

[15] X. Wang, C. Yang, and S. Mao, "PhaseBeat: Exploiting CSI phase data for vital sign monitoring with commodity WiFi devices," in *Proc. IEEE ICDCS 2017*, Atlanta, GA, June 2017, pp. 1230–1239.

[16] X. Wang, C. Yang, and S. Mao, "On CSI-based vital sign monitoring using commodity WiFi," *ACM Transactions on Computing for Healthcare*, to appear, DOI: 10.1145/3377165.

[17] X. Wang, C. Yang, and S. Mao, "Tensorbeat: Tensor decomposition for monitoring multiperson breathing beats with commodity wifi," *ACM Transactions on Intelligent Systems and Technology*, vol. 9, no. 1, pp. 8:1–8:27, Sept. 2017.

[18] H. Wang, D. Zhang, J. Ma, Y. Wang, Y. Wang, D. Wu, T. Gu, and B. Xie, "Human respiration detection with commodity WiFi devices: Do user location and body orientation matter?" in *Proc. Ubicomp'16*, Heidelberg, Germany, Sept. 2016, pp. 25–36.

[19] Z. Yang, Z. Zhou, and Y. Liu, "From RSSI to CSI: Indoor localization via channel response," *ACM Computing Surveys*, vol. 46, no. 2, pp. 25:1–25:32, Nov. 2013.

[20] W. Wang, A. X. Liu, M. Shahzad, K. Ling, and S. Lu, "Understanding and modeling of WiFi signal based human activity recognition," in *Proc. ACM MobiCom 2015*, Paris, France, Sept. 2015, pp. 65–76.

[21] J. Gjengset, J. Xiong, G. McPhillips, and K. Jamieson, "Phaser: Enabling phased array signal processing on commodity WiFi access points," in *Proc. ACM Mobicom'14*, Maui, HI, Sept. 2014, pp. 153–164.

[22] S. Roberts, "Control chart tests based on geometric moving averages," *Technometrics*, vol. 42, no. 1, pp. 97–101, 2000.

[23] NeuLog Sensors, "Respiration Monitor Belt logger sensor NUL-236," 2020 (accessed March 6, 2020). [Online]. Available: https://neulog.com/respiration-monitor-belt/

[24] Y. Zeng, D. Wu, J. Xiong, E. Yi, R. Gao, and D. Zhang, "FarSense: Pushing the range limit of WiFi-based respiration sensing with CSI ratio of two antennas," *Proceedings of the ACM on Interactive, Mobile, Wearable and Ubiquitous Technologies*, vol. 3, no. 3, pp. 1–26, Sept. 2019.

[25] Y. Zeng, E. Yi, D. Wu, R. Gao, and D. Zhang, "A CSI-ratio model based house-level respiration monitoring system using COTS WiFi devices," in *Proc. ACM UbiComp/ISWC'19*, London, UK, Dec. 2010, pp. 354–357.

[26] Y. Zeng, E. Yi, D. Wu, R. Gao, and D. Zhang, "A full human respiration detection system using commodity Wi-Fi devices," in *Proc. UbiComp/ISWC'18*, Singapore, Dec. 2018, pp. 480–483.
[27] Y. Hou, Y. Wang, and Y. Zheng, "TagBreathe: Monitor breathing with commodity RFID systems," in *Proc. IEEE ICDCS 2017*, Atlanta, GA, June 2017, pp. 404–413.
[28] C. Yang, X. Wang, and S. Mao, "AutoTag: Recurrent vibrational autoencoder for unsupervised apnea detection with RFID tags," in *Proc. IEEE GLOBECOM 2018*, Abu Dhabi, United Arab Emirates, Dec. 2018, pp. 1–7.
[29] C. Yang, X. Wang, and S. Mao, "Unsupervised detection of apnea using commodity RFID tags with a recurrent variational autoencoder," *IEEE Access Journal*, vol. 7, no. 1, pp. 67 526–67 538, June 2019.
[30] Y. Wang, J. Liu, Y. Chen, M. Gruteser, J. Yang, and H. Liu, "E-eyes: Device-free location-oriented activity identification using fine-grained wifi signatures," in *Proc. ACM Mobicom'14*, Maui, HI, Sept. 2014, pp. 617–628.
[31] G. Wang, Y. Zou, Z. Zhou, K. Wu, and L. M. Ni, "We can hear you with Wi-Fi!" *IEEE Trans. Mobile Comput.*, vol. 15, no. 11, pp. 2907–2920, Dec. 2016.
[32] S. Tan and J. Yang, "WiFinger: Leveraging commodity WiFi for fine-grained finger gesture recognition," in *Proc. ACM MobiHoc 2016*, Paderborn, Germany, July 2016, pp. 201–210.
[33] A. Virmani and M. Shahzad, "Position and orientation agnostic gesture recognition using WiFi," in *Proc. ACM MobiSys 2017*, Niagara Falls, June 2017, pp. 252–264.
[34] K. Ali, A. X. Liu, W. Wang, and M. Shahzad, "Recognizing keystrokes using WiFi devices," *IEEE J. Sel. Areas Commun.*, vol. 35, no. 5, pp. 1175–1190, May 2017.
[35] Y. Zeng, P. H. Pathak, and P. Mohapatra, "WiWho: WiFi-based person identification in smart spaces," in *Proc. IEEE IPSN 2016*, Vienna, Austria, Apr. 2016, pp. 1–12.
[36] W. Xi, J. Zhao, X.-Y. Li, K. Zhao, S. Tang, X. Liu, and Z. Jiang, "Electronic frog eye: Counting crowd using WiFi," in *Proc. IEEE INFOCOM 2014*, Toronto, Canada, Apr./May 2014, pp. 361–369.
[37] C. Shi, J. Liu, H. Liu, and Y. Chen, "Smart user authentication through actuation of daily activities leveraging WiFi-enabled IoT," in *Proc. ACM MobiHoc 2017*, Chennai, India, July 2017, pp. 1–10.
[38] S. Doong, "Counting human flow with deep neural network," in *Proc. HICSS 2018*, Waikoloa Village, HI, Jan. 2018, pp. 799–808.
[39] K. Qian, C. Wu, Z. Yang, Y. Liu, and Z. Zhou, "PADS: Passive detection of moving targets with dynamic speed using PHY layer information," in *Proc. 20th IEEE International Conference on Parallel and Distributed Systems (ICPADS)*, Hsinchu, Taiwan, Dec. 2014, pp. 1–8.
[40] Y. Wang, K. Wu, and L. M. Ni, "Wifall: Device-free fall detection by wireless networks," *IEEE Trans. Mobile Comput.*, vol. 16, no. 2, pp. 581–594, Feb. 2017.
[41] S. Zhong, Y. Huang, R. Ruby, L. Wang, Y.-X. Qiu, and K. Wu, "Wi-fire: Device-free fire detection using WiFi networks," in *Proc. IEEE ICC 2017*, Paris, France, May 2017, pp. 1–6.
[42] X. Wang, J. Zhang, Z. Yu, S. Mao, S. Periaswamy, and J. Patton, "On remote temperature sensing using commercial UHF RFID tags," *IEEE Internet of Things Journal*, vol. 6, no. 6, pp. 10 715–10 727, Dec. 2019.
[43] W. Yang, X. Wang, A. Song, and S. Mao, "Wi-Wheat: Contact-free wheat moisture detection using commodity WiFi," in *Proc. IEEE ICC 2018*, Kansas City, MO, May 2018, pp. 1–6.
[44] W. Yang, X. Wang, S. Cao, H. Wang, and S. Mao, "Multi-class wheat moisture detection with 5GHz Wi-Fi: A deep LSTM approach," in *Proc. ICCCN 2018*, Hangzhou, China, July/Aug. 2018, pp. 1–9.
[45] X. Wang, L. Gao, S. Mao, and S. Pandey, "CSI-based fingerprinting for indoor localization: A deep learning approach," *IEEE Trans.Veh. Technol.*, vol. 66, no. 1, pp. 763–776, Jan. 2017.
[46] X. Wang, L. Gao, and S. Mao, "CSI phase fingerprinting for indoor localization with a deep learning approach," *IEEE Internet of Things Journal*, vol. 3, no. 6, pp. 1113–1123, Dec. 2016.
[47] X. Wang, L. Gao, and S. Mao, "BiLoc: Bi-modal deep learning for indoor localization with commodity 5Ghz WiFi," *IEEE Access Journal*, vol. 5, pp. 4209–4220, Mar. 2017.
[48] M. Kotaru, K. Joshi, D. Bharadia, and S. Katti, "SpotFi: Decimeter level localization using WiFi," in *Proc. ACM SIGCOMM 2015*, London, UK, Aug. 2015, pp. 269–282.

Xuyu Wang [S'13-M'18] received the M.S. in Signal and Information Processing in 2012 and B.S. in Electronic Information Engineering in 2009, both from Xidian University, Xi'an, China. He received a Ph.D. in Electrical and Computer Engineering from Auburn University, Auburn, AL, USA in Aug. 2018. He is an Assistant Professor in the Department of Computer Science, California State University, Sacramento, CA. His research interests include indoor localization, deep learning, and big data. He received a Woltolsz Fellowship at Auburn University, and is a co-recipient of the Second Prize of Natural Scientific Award of Ministry of Education, China in 2013, the Best Paper Award of IEEE GLOBECOM 2019, The Best Journal Paper Award of IEEE Communications Society Multimedia Communications Technical Committee in 2019, the Best Demo Award of IEEE SECON 2017, and the Best Student Paper Award of IEEE PIMRC 2017.

Chao Yang [S'18] received the B.S. degree in electrical engineering from Yanshan University, He'bei, China in 2015, and an MS degree in Electrical and Computer Engineering (ECE) from Auburn University, Auburn, AL in 2017. He has been pursuing a PhD in ECE at Auburn University since Spring 2018. His current research interests include health sensing, indoor localization, internet of Things and wireless networks. He is a co-recipient of the Best Paper Award of IEEE GLOBECOM 2019.

Shiwen Mao [S'99-M'04-SM'09-F'19] received his Ph.D. in electrical and computer engineering from Polytechnic University, Brooklyn, NY. Currently, he is the Samuel Ginn Professor in the Department of Electrical and Computer Engineering, and Director of the Wireless Engineering Research and Education Center (WEREC) at Auburn University, Auburn, AL. His research interests include wireless networks, multimedia communications, and smart grid. He is on the Editorial Board of IEEE Transactions on Wireless Communications, IEEE Transactions on Network Science and Engineering, IEEE Transactions on Mobile Computing, IEEE Internet of Things Journal, IEEE Multimedia, IEEE Networking Letters, and ACM GetMobile, among others. He received the IEEE ComSoc TC-CSR Distinguished Technical Achievement Award in 2019 and NSF CAREER Award in 2010. He is a co-recipient of the IEEE ComSoc MMTC Best Conference Paper Award in 2018, the Best Demo Award from IEEE SECON 2017, the Best Paper Awards from IEEE GLOBECOM 2019, 2016 & 2015, IEEE WCNC 2015, and IEEE ICC 2013, and the 2004 IEEE Communications Society Leonard G. Abraham Prize in the Field of Communications Systems. He is a Fellow of the IEEE.